Reductive immobilization of ^{99}Tc(VII) by FeS_2: The effect of marcasite

Diana M. Rodríguez [a], Natalia Mayordomo [a,*], Dieter Schild [b], Salim Shams Aldin Azzam [a], Vinzenz Brendler [a], Katharina Müller [a,**], Thorsten Stumpf [a]

[a] Helmholtz-Zentrum Dresden – Rossendorf (HZDR), Institute of Resource Ecology, Bautzner Landstraße 400, 01328, Dresden, Germany
[b] Karlsruhe Institute of Technology (KIT), Institute for Nuclear Waste Disposal, Hermann-von-Helmholtz-Platz 1, 76344, Eggenstein-Leopoldshafen, Germany

ARTICLE INFO

Handling Editor: Milena Horvat

Keywords:
Technetium removal
Iron sulfide
Iron sulfate
Pyrite
Remediation

ABSTRACT

Reductive immobilization of ^{99}Tc by a synthetic FeS_2 mixture, i.e. marcasite-pyrite 60:40, was studied by a combined approach of batch experiments and powder X-ray diffraction, X-ray photoelectron spectroscopy as well as Raman microscopy. It was found that the FeS_2 mixture removes 100% of Tc from the suspension after 7 days in contact at $6.0 < pH \leq 9.0$. The retention outside that pH range was slower and incomplete. Spectroscopic analysis showed that the redox active species at pH 6.0 is Fe^{2+} as expected from previous works with pyrite. However, at pH 10.0 the surprising oxidation of S^{2-} to SO_4^{2-} was found responsible for Tc immobilization. This was explained by the high reactivity of marcasite that is easily oxidized to produce H_2SO_4. Our work provides new molecular insights into the reductive mobilization of Tc(VII) by oxidative formation of sulfate. The assigned molecular reactions may also be relevant for the assessment of other redox reactive contaminants. Technetium re-oxidation experiments showed that the fast oxidation of marcasite is associated to the reduction of the remaining Tc(VII) in solution, which gives marcasite the potential of Tc natural remediation since it delays the re-oxidation of Tc(IV).

1. Introduction

Technetium (Tc, Z 43) was discovered in Italy by Perrier and Sagré in 1937 (Perrier and Segrè, 1937). Its application as a clinical tracer element was first published in the early 60's (Herbert et al., 1965). Since then, the metastable ^{99m}Tc (half-life of 6.007 h) has been used for the detection of tumors, as well as for the imaging of several organs like the brain or the liver. Despite its relevance in medicine, technetium is very problematic from the environmental point of view. The primary isotope, i.e. ^{99}Tc, a pure β^- emitter with a half-life of 2.14×10^5 years, is produced with a high yield of 6% during the fission of ^{235}U and ^{239}Pu (Meena and Arai, 2017). Even though it may be naturally formed in trace amounts through the spontaneous fission of ^{238}U or the interaction of cosmic rays with molybdenum, ruthenium and niobium present in the Earth crust, the vast majority of the technetium present on our planet originates from human activities, like nuclear power production (Meena and Arai, 2017; Icenhower et al., 2010).

In addition to its long half-life, complex ^{99}Tc speciation adds to its high environmental risk. Under oxidizing conditions it is mainly occurring as pertechnetate, $Tc(VII)O_4^-$, an anion that is practically not sorbed by minerals or sediments, and also does not form insoluble compounds (Lieser and Bauscher, 1987). Thus, it freely migrates within ground water (Meena and Arai, 2017; Icenhower et al., 2010). If Tc reaches the biosphere, it will be rapidly incorporated into the food chain and when Tc dose exceeds 0.04 mSv per year (equivalent to the intake of 182 μg of Tc), it can increase the risk of cancer as well as other health problems related to radiation exposure (Environmental Protection Agency, 2000). Therefore, establishing strategies for pertechnetate immobilization and remediation is of great importance for the nuclear waste management and environmental protection. The most stable species under reducing conditions is $Tc(IV)O_2$, a scarcely soluble oxide with a very low mobility. Consequently, a reduction of TcO_4^- to TcO_2 is the most viable strategy for technetium immobilization (Meena and Arai, 2017; Pearce et al., 2019; Gu et al., 2018). Several minerals containing different reducing moieties like Sn(II) (Levitskaia et al., 2016; Johnson et al., 2018) or Fe(II) (Yalçıntaş et al., 2016a; Mayordomo et al., 2020; Lee et al., 2016; Boglaienko and Levitskaia, 2019; Boglaienko et al., 2021) have been proven to effectively scavenge Tc from solution through the formation of Tc(IV) and its consecutive precipitation, sorption and/or incorporation.

Pyrite, cubic iron sulfide (FeS_2), has shown a remarkable ability for the

* Corresponding author.
** Corresponding author.
E-mail addresses: n.mayordomo-herranz@hzdr.de (N. Mayordomo), k.mueller@hzdr.de (K. Müller).

remediation of pollutants such as mercury (Sun et al., 2017), chromium (Wang et al., 2019; Li et al., 2020) and molybdenum (Xu et al., 2006). In a recent study, we have found that it removes almost 100% of Tc(VII) from solution after one day in contact at $5.5 \leq pH \leq 10.5$ (Rodríguez et al., 2020). X-ray absorption spectroscopy, XAS, showed that after the reduction from Tc (VII), Tc(IV) was either sorbed onto hematite (α-$Fe(III)_2O_3$) at pH 6.0 or incorporated into magnetite ($Fe(II)Fe(III)_2O_4$) at pH 10.0, with both hematite and magnetite being oxidation products of pyrite. Based on these results, we concluded that natural attenuation of Tc is expected in nuclear waste repositories with clays (namely bentonite) used as backfill materials, where pyrite is a very common accessory mineral (Bildstein et al., 2006; De Craen et al., 2004; Gaucher et al., 2004). This is in particular relevant in sites like the Onkalo spent nuclear fuel repository, where pyrite is abundant per se (Talikka, 2005). However, these natural attenuation effects clearly depend on the interaction between technetium and other minerals present, possibly changing the retention of Tc. Thus, more realistic scenarios like the presence of marcasite, a FeS_2 polymorph commonly found along with pyrite in the environment (Yao et al., 2020), should be taken into account. Even though both minerals crystallize in different crystal systems, i.e. orthorhombic (marcasite) and cubic (pyrite) and have different space groups (marcasite: Pnnm; pyrite: $Pa\bar{3}$), they are commonly misidentified and confused based on mere crystal habit. For example, acicular pyrite crystals are considered marcasite while in applications like jewelry it is very frequent that pyrite is sold as marcasite (Rickard, 2012).

It has been proven that polymorphism, i.e. the existence of a solid phase in different crystalline structures, has a significant effect on the retention of pollutants by minerals. One example is europium sorption that is faster on γ-alumina (γ-Al_2O_3) than on corundum (α-Al_2O_3) because the reaction rates are influenced by the crystallographic features of the mineral (Baumer and Hixon, 2018). The same effect has been observed for plutonium sorption on hematite and maghemite (γ-Fe_2O_3) (Khasanova et al., 2007). Thus, it is quite probable that the retention of pollutants by natural pyrite is affected by the presence of marcasite; however, no studies addressed this so far. More specifically for technetium, retained Tc(IV) might get re-mobilized after the decomposition of marcasite, that is unstable with respect to pyrite and whose main oxidation product, H_2SO_4, is a potential re-oxidation agent for Tc(IV). Therefore, in order to design an efficient remediation strategy for Tc, a basic understanding of the effect of marcasite on Tc immobilization by pyrite is needed.

In this work, we have studied the retention of Tc(VII) by a well characterized synthetic mixture of marcasite-pyrite 60:40 using a combined approach of batch experiments with spectroscopic and diffraction measures. The batch contact experiments were carried out at pH ranging from 4.0 to 10.5, contact times from 1 to 45 days, and Tc concentrations varying from 0.1 μM to 1 mM. X-ray photoelectron spectroscopy (XPS), Raman microscopy and powder X-ray diffraction (XRD) were applied to the Tc loaded solids to determine oxidation states and the mineralogical changes after the interaction with technetium. Additionally, re-oxidation experiments were performed at pH 6.0 and 10.0 for 90 days, where Raman microscopy and XRD identified the reaction products.

2. Materials and methods

Radiation safety. ^{99}Tc is a β-particle emitter and should be handled only in a dedicated radiochemistry laboratory with specific radiation safety protocols in place.

General notes. Unless indicated otherwise, all preparations were performed under N_2 atmosphere inside a glovebox (GS Glovebox-System GS050912; <1 ppm O_2) at 21 °C. The Milli-Q water (resistivity of 18.2 MΩ cm, Water Purified®) used for the experiments was boiled for 2 h for degassing, sealed and cooled down to room temperature before its placement into the glovebox.

The Eh was measured with an Eh electrode (Inlab redox micro 51343203, Mettler Toledo) calibrated with a redox buffer solution (220 mV/pH 7). The pH was measured by using a pH meter (pH3110, WTW) with a pH electrode (SI Analytics Blue Line) calibrated with standard pH buffers 4.006, 6.865 and 9.180 (WTW).

2.1. Mineral synthesis and characterization

Iron sulfide, FeS_2, was synthesized in a Schlenk line following the procedure described by Huo et al. (2017) Briefly, 200 mL of 0.1 M $FeCl_3$ and 200 mL of 0.2 M NaHS were prepared and purged with N_2 for 30 min. Then, the solutions were mixed in a round flask of 500 mL and left under N_2 atmosphere and constant stirring for another 30 min. Lastly, the mixture was sealed and aged for 24 h in a stove at 60 °C. The black powder obtained was separated by ultracentrifugation (Optima XPN-80 Ultracentrifuge, Beckman Coulter at $2.4 \times 10^5 \times g$ for 1 h, these conditions apply for all centrifugations) and dried by lyophilization.

The characterization of the mineral is presented in the Supporting Information (Fig. S1). It was done by powder XRD (MiniFlex 600 powder XRD, Rigaku) using Cu Kα (λ 1.54184 Å) as X-ray source with an X-ray generation of 40 kV/15 mA (600 W) and a D/teX Ultra 1D silicon strip detector in the Bragg-Brentano θ-2 θ geometry at a scanning speed of 0.02 deg per min. The samples were prepared inside the glovebox, using an agate mortar to homogenize the solid and placing it into a Kapton tape capped low-background airtight sample holders (Rigaku) to ensure inert N_2 conditions. The Brunauer-Emmett-Teller specific surface area was determined as $5.3 \pm 0.4\ m^2\ g^{-1}$, using isotherm experiments with N_2 at 77 K (Multipoint Beckman Coulter surface analyzer SA 3100). The isoelectric point of the mineral (pH_{IEP}) was determined by zeta potential experiments (Zetasizer Nano Series Nano-ZS, Malvern Instruments) of 0.05 g L^{-1} mineral suspensions in 0.1 M NaCl at pH values between 3.0 and 10.5. Each sample was scanned for 30 s; the data presented here are averages of five independent scans. Scanning electron microscopy (SEM) was used to analyze the mineral morphology. The sample was prepared inside the anoxic glovebox and moved by a shuttle (Leica VCT) under inert conditions into the environmental scanning electron microscope (FEI Quanta 650 FEG, now Thermo Fisher Inc.). The operating voltage was 30 kV and the pressure in the analysis chamber 2.8×10^{-4} Pa.

2.2. Batch sorption experiments

All batch experiments started with the preparation of suspensions of the mixture marcasite-pyrite 60:40, from now on simply referred to synthesized FeS_2. In general, 42.6 mg of synthesized FeS_2 were suspended in water or 0.1 M NaCl ($NaCl_{(s)}$ from Merck, purity ≥ 99%) depending on the experiment. Afterwards, the indicated amount of a 9.22×10^{-3} M $K^{99}TcO_4$ stock solution (Institute of Radiopharmaceutical Cancer Research, HZDR) was added. The final volume of the sample was 32 mL (final solid to liquid ratio 1.3 ± 0.2 g L^{-1}). The pH of the samples was adjusted with solutions from 1 to 0.02 M of HCl or NaOH. Due to the oxidation of FeS_2 (Bonnissel-Gissinger et al., 1998), the pH was adjusted regularly every 3–4 days adding small amounts of HCl or NaOH if required. Such additions never exceeded 10 μL to ensure constant Tc concentration and ionic strength in the sample.

Once the pH was adjusted, the samples were placed on a horizontal shaker for agitation for the required contact time. After this, the stirring was stopped and the pH and Eh were measured (equilibrium time for Eh measure: 30 min). Table S1 in the supporting information (SI) summarizes the conditions for the batch experiments.

The samples were then ultracentrifuged and 250 μL aliquots from the supernatant were taken to measure the remaining Tc concentration by liquid scintillation counting, LSC (1414 LSC Winspectral α/β Wallac, PerkinElmer; detection limit: 0.42 Bq; measuring time: 10 min).

The amount of Tc retained by the synthesized FeS_2 ($\%Tc_{removed}$) was calculated as follows:

$$\%Tc_{removed} \quad \frac{([Tc]_0 \quad [Tc]_t)}{[Tc]_0} \times 100 \qquad \text{Eq.1}$$

where $[Tc]_0$ is the initial Tc concentration in the system (in Bq mL^{-1}), measured in a blank solution without the solid, and $[Tc]_t$ is the concentration of Tc remaining in solution after contact with the synthesized FeS_2 (in Bq mL^{-1}) after certain time (t) of contact.

2.3. X-ray photoelectron spectroscopy (XPS)

0.140 g of the synthesized FeS_2 were transferred into 50 mL of water and the required amount of $K^{99}TcO_4$ was added to obtain ≈1000 ppm of Tc load in the final solid (Tc initial concentration 0.048 mM). Such concentration was necessary achieve at least 4 Tc atoms nm^{-2}, which is the value needed to perform measurements. The pH was adjusted to 6.0 and 10.0 and the samples were left for equilibration for a month on a horizontal shaker (the pH was also adjusted twice a week during this month). Afterwards, the solid was separated by ultracentrifugation and the supernatant was removed. The wet paste was re-dissolved in ≈1 mL of water. Two blanks of synthesized FeS_2 suspensions in water (1.3 g L^{-1}) were prepared at pH 6.0 and 10.0, left in horizontal stirring for one month adjusting the pH occasionally. They were measured at the same conditions as the ^{99}Tc-loaded samples. The samples were always transported and measured under inert gas atmosphere (N_2 and Ar).

A drop of the suspension was applied on indium foil and left to dry. Afterwards, the samples were moved into the XPS (PHI 5000 VersaProbe II, ULVAC-PHI Inc.) using an airtight transfer vessel. The XPS is equipped with a scanning microprobe X-ray source (monochromatic Al Kα (1486.7 eV) X-rays). X-ray source power of 32 W and pass energy of the analyzer of 187.85 eV were used to perform survey scans of the conductive samples. Narrow scans of the elemental lines were recorded at 23.5 eV pass energy, yielding an energy resolution of 0.67 eV FWHM at the Ag $3d_{5/2}$ elemental line of pure silver. The binding energies of elemental lines of pure metals (monochromatic Al K_α: Cu $2p_{3/2}$ at 932.62 eV, Au $4f_{7/2}$ at 83.96 eV) (Seah et al., 1998) were used for the calibration of the binding energy scale of the spectrometer, obtaining an estimated error of ±0.2 eV.

2.4. Raman microscopy

Two suspensions of 1.3 ± 0.2 g L^{-1} of the synthesized FeS_2 were prepared in water and their pH was adjusted to 6.0 and 10.0. The required amount of $K^{99}TcO_4$ was added to obtain ≈100 ppm of Tc load in the final solid (Tc initial concentration 5 μM). Tc and the samples were placed on the horizontal shaker for two weeks with regular pH adjustments. Afterwards, the solids were separated by ultracentrifugation and distributed for Raman microscopy and powder XRD.

The wet paste was deposited on a cell containing two CaF_2 Raman quality windows (Mayordomo et al., 2020). Once the solid was dry, the cell was sealed to ensure inert atmosphere during the measure. Raman microscopy (Aramis, Horiba) was performed using a He – Ne laser (wavelength: 532 nm) with a 10-fold objective with a D 0.3 filter, a pin-hole of 500 μm and a slit of 600 μm.

2.5. Re-oxidation

Two suspensions of the synthesized FeS_2 in water (1.3 ± 0.2 g L^{-1}) were prepared inside the glovebox at pH 6.0 and 10.0, both containing 5 μM $K^{99}TcO_4$ (50 mL polypropylene tubes yielding a final volume of 35 mL). They were agitated for 14 days during which the pH was regularly adjusted as in the batch experiments (section 2.2). Subsequently, 3 mL aliquots of each sample were ultracentrifuged and the supernatant was sampled for determination of Tc concentration remaining in solution by LSC (section 2.2).

The tubes were opened outside the glovebox (under ambient atmosphere) and left with constant stirring for 1 h. Afterwards they were closed and placed on a horizontal shaker outside the glovebox for 64 days. Identically to the batch experiments, we tried to adjust the pH, but this was not possible as it always dropped to ~3 due to the production of H_2SO_4 after the oxidation of the mineral (Bonnissel-Gissinger et al., 1998) independent of the initial pH (6.0 or 10.0). Therefore, after two weeks adjusting every day, we decided not to adjust the pH anymore but leave it at the stable value reached after the interaction with oxygen (pH 3.0 instead of 6.0 and pH 2.8 instead of 10.0).

The suspensions were regularly sampled by taking 3 mL aliquots to measure the Tc remaining in the supernatant by LSC (section 2.2). The solids obtained after 60 days of the re-oxidation experiments were studied by powder XRD and Raman microscopy (sections 2.1 and 2.4).

2.6. Speciation calculations

Calculations were performed using the code Chess V2.4 (van der Lee and de Wint, 1999). The most recent Nuclear Energy Agency thermodynamic databases for Fe (Lemire et al., 2013, 2019) and Tc (Grenthe et al., 2020) and their recommended S thermodynamic data were used.

The reduction of 5 μM Tc(VII) by either S^{2-} or Fe^{2+} was studied as a function of pH. All calculations assumed that the Tc(VII) reduction was promoted by either dissolved Fe^{2+} or S^{2-} at 25 °C with no gas dissolution. It was considered that 1% of 1.3 g L^{-1} FeS_2 was dissolved, i.e. 0.1 mM Fe^{2+} and 0.2 mM S^{2-}. However, it has to be kept in mind that this assumption might not represent a realistic scenario since Tc(VII) reduction is promoted by the structural S^{2-} or Fe^{2+}, whose redox potentials differ from the dissolved ones when they form part of a mineral structure (Gorski et al., 2016; Li et al., 2009).

3. Results and discussion

3.1. Batch sorption experiments

Fig. 1 shows the results of the batch experiments performed to study the ^{99}Tc(VII) uptake by the synthesized FeS_2 as a function of Tc concentration, time and pH.

The isotherm at pH 6.5 (Fig. 1a) shows that the lower the Tc concentration in suspension, the better its removal by the synthesized FeS_2. These results are especially important because, due to technical reasons, for analyzing the kinetics of the removal process as well as the pH effect, we have used a Tc concentration of 5 μM, which is three orders of magnitude higher than the typical technetium concentration in the environment (1×10^{-9} M) (Schulte and Scoppa, 1987; Shi et al., 2012). Therefore, the isotherm serves as a proof-of-concept of our experiments. Additionally, the isotherm shows a slope of 0.5 suggesting a single reaction mechanism, i.e. sorption on one site. This slope value indicates either that the affinity of the mineral for the technetium is low (Limousin et al., 2007), or that the mechanism of removal could be the precipitation of Tc(IV), most probably as TcO_2 or a TcS_x species (Rard et al., 1999).

The kinetics of the Tc uptake at pH 6.5 are represented in Fig. 1b. It can be seen that Tc removal increases with time, with 50% of the initial technetium removed after one day in contact with the synthesized FeS_2. 100% of Tc(VII) uptake was reached after 7 days. The experiment was carried out for 45 days and the percentage of Tc(VII) scavenged was constant, showing no re-mobilization of the radionuclei. Compared with the Tc immobilization by pure pyrite (Rodríguez et al., 2020), the presence of marcasite slows down the process, since pure pyrite removed 100% of Tc already after one day of contact under the same conditions.

Fig. 1c shows that the removal of Tc(VII) from water at $6.0 < pH \leq 9.0$ is close to 100%. Under more acidic conditions, the scavenging of technetium by the synthesized FeS_2 is less effective because the solubility of FeS_2 increases as the pH decreases (King, 2013). It has been found that the heterogeneous reduction of Tc(VII) by Fe(II) is more effective than the homogenous reduction (i.e. in solution) since when Fe^{2+} as reducing agent is in solution the formation of Tc(IV) is kinetically hindered (Cui and Eriksen, 1996a). In contrast, the reduction becomes more prominent when the Fe(II) takes part of a mineral structure (Huo et al.,

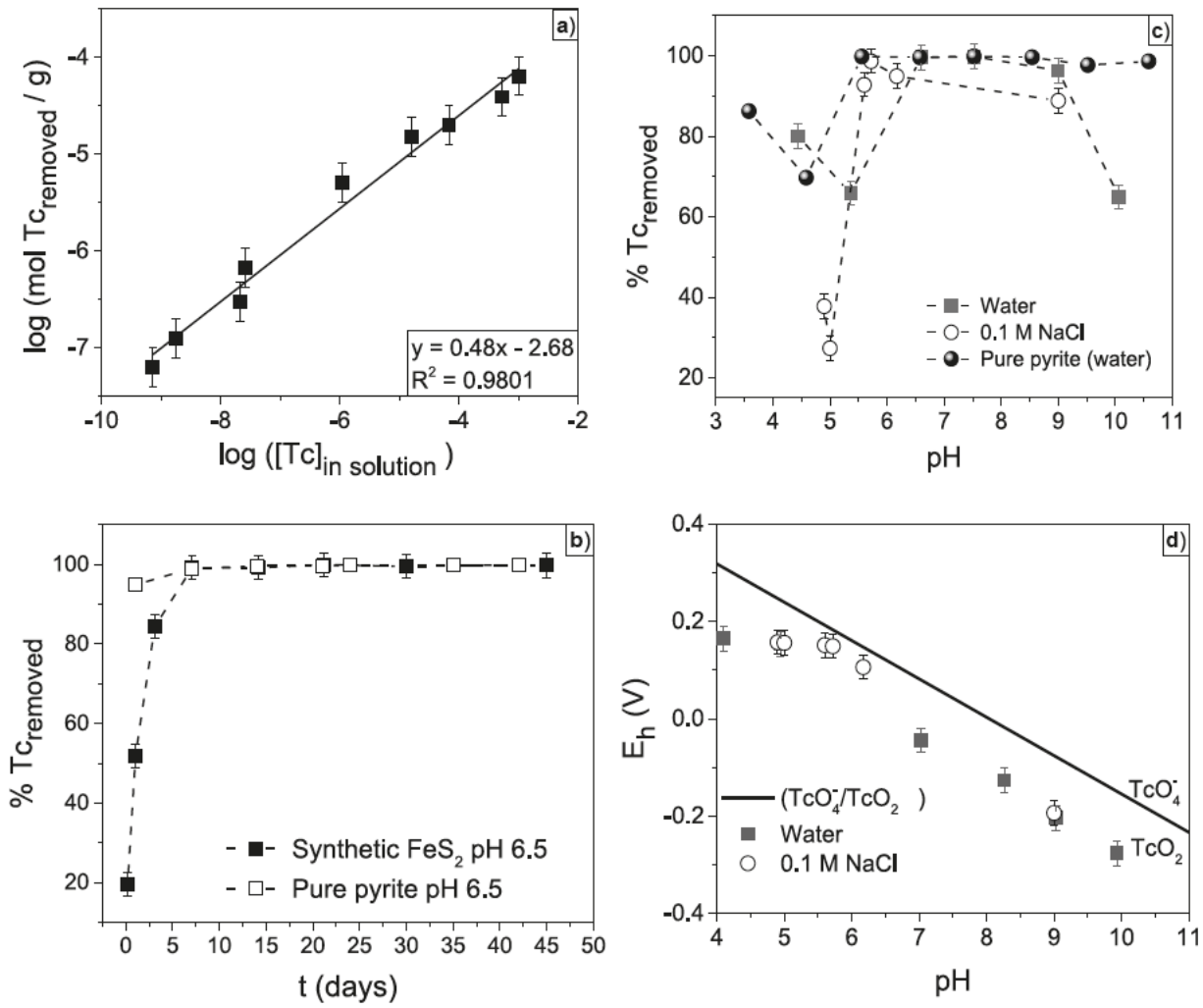

Fig. 1. Batch experiments of ^{99}Tc(VII) removal by synthetic FeS_2. a) Isotherm at pH 6.5 in water after 14 days of contact. b) Scavenging kinetics at pH 6.5 in water. Tc removal by pure pyrite at pH 6.0 in water was added for comparison (Rodríguez et al., 2020). **c) Impact of ionic strength: water vs 0.1 M NaCl after 14 days in contact. Tc removal by pure pyrite in water for 14 days was added for comparison (Rodríguez et al., 2020). d) Pourbaix diagram of the samples of c. Dashed lines in b and c are shown to guide the eye.**

2017; Cui and Eriksen, 1996a, 1996b; Zachara et al., 2007), or when it is pre-sorbed on a reactive mineral surface like on alumina (Mayordomo et al., 2020). In our work, Tc removal at pH < 6.0 decreases due to FeS_2 dissolution, which hinders Tc(VII) reduction.

The Tc uptake by the synthesized FeS_2 also becomes lower at pH 10.0, which might be a result of an increased solubility of TcO_2 (Yalçıntaş et al., 2016a; Baumann et al., 2018), or the formation of TcS_x–like compounds on the surface that would passivate the mineral, preventing a further Tc reduction (Pearce et al., 2018). It has been reported that technetium can passivate iron containing materials by forming layers of technetium oxides (Cartledge, 1955, 1971), however, in our previous study of Tc retention by pure pyrite (Rodríguez et al., 2020) such effect was not observed at pH 10.0 when technetium interacted solely with oxygen, which lead us to conclude that if passivation is indeed taking place, it would be most likely due to the formation of TcS_x and not TcO_2. The Pourbaix diagram (Fig. 1d) confirms the reduction from Tc(VII) to Tc(IV) in the whole pH range studied, making the formation of both TcO_2 or TcS_x equally possible. One additional hint for a molecular process understanding is given by the addition of 0.1 M NaCl to the retention system (Fig. 1c). As a consequence, the Tc removal at 6.0 < pH ≤ 9.0 does not significantly change, meaning that inner-sphere complexation is likely taking place (Hiemenz and Rajagopalan, 1997). The difference on the Tc scavenging at pH < 6.0 between the system in water and 0.1 M NaCl can be explained either by outer-sphere complexation or by the increase on Tc (IV) solubility as the ionic strength increases (Yalçıntaş et al., 2016a; Hess et al., 2004). In case that Tc(IV) is in solution, its interaction with the synthesized FeS_2 would be hindered due to their charge repulsion. Although batch experiments provided important macroscopic information, a combined approach of spectroscopic and diffraction methods is needed for conclusions on the chemical identity of the Tc species formed at the synthetic FeS_2 – water interface.

3.2. *Molecular analysis of Tc loaded solids*

To gain understanding on the retention on a molecular level, Raman microscopy and XPS were performed on the solid samples after the interaction with technetium. The Raman spectra of the solids at pH 6.0 and 10.0 are presented in Fig. 2. At pH 6.0 the formation of hematite as the resulting iron phase after the FeS_2 oxidation is confirmed by comparison of the spectra with the reference R050300 of the RRUFF database (Lafuente et al., 2016). This result is in good agreement with our previous findings with pyrite (Rodríguez et al., 2020), where the inner-sphere complexation of Tc(IV)-Tc(IV) dimers with hematite was responsible of the Tc removal from solution at pH 6.0.

Unlike the removal with pure pyrite (Rodríguez et al., 2020), the Raman spectra of the solid at pH 10.0 presents a band at 993 cm^{-1}

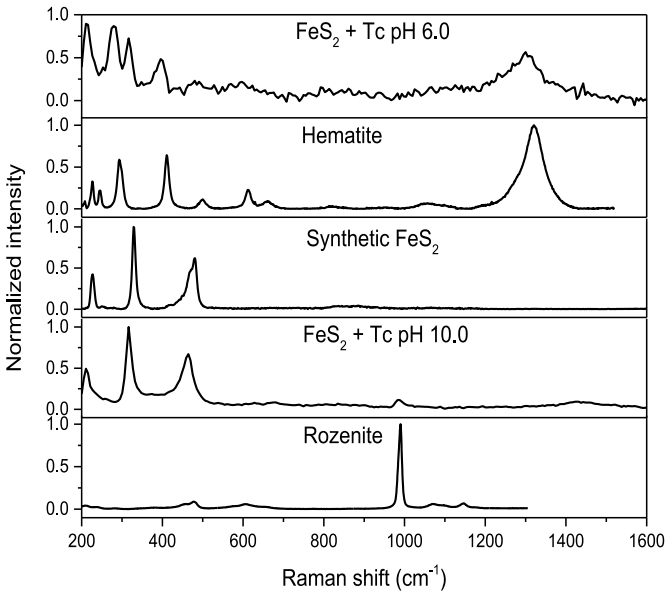

Fig. 2. Raman spectra of Tc loaded (100 ppm) synthetic FeS_2 samples at pH 6.0 and pH 10.0. The spectra of the pure synthetic FeS_2 sample and reference spectra of hematite (reference R050300) and rozenite ($FeSO_4 \times 4H_2O$, reference R070187) are shown for comparison (Lafuente et al., 2016).

typical for the sulfate group of several Fe(II)-sulfate-hydrate minerals. As a reference rozenite ($Fe(II)SO_4 \times 4H_2O$) is shown in Fig. 2. This band would indicate that the oxidation reaction at this pH value is not that of iron, as expected for the Tc(VII) reductive immobilization, but of sulfur. This is supported by the high spectral similarity of the Raman spectra of the Tc loaded FeS_2 at pH 10.0 with the pure synthetic FeS_2. The band around 478 cm^{-1} present in the synthesized FeS_2 before and after the interaction with technetium can be assigned to the Fe(III) moieties (Hanesch, 2009) described in the mineral characterization presented in the Supporting Information.

Fig. 3 shows the XPS spectra evaluated for Fe *2p*, S *2p*, O *1s*, and Tc *3d*. Fig. 3a illustrates the formation of Fe(III) at pH 6.0. In contrast, there is no significant change indicating the oxidation of iron at pH 10.0. This supports the interpretation of Raman spectra (Fig. 2) and confirms that at pH 10.0 the main redox sensitive element of the synthesized FeS_2 is sulfur. However, the S *2p* spectra (Fig. 3b) at pH 10.0 show no signal for sulfate, expected around 168 eV, whereas the binding energies of Fe $2p_{3/2}$ (707.2 eV) and S $2p_{3/2}$ (162.5 eV) can be unequivocally assigned to FeS_2. This can be explained by a significantly lower sulfate concentration below the XPS detection limit concentration as result of the incomplete reduction of 5 μM Tc. Whereas XPS analyzes the sample as a whole, the Raman microscope records spectra from different regions of interest of the mineral, being able to detect minor components. As the formation of sulfate is the result of the heteroreduction of technetium, it becomes clear why it could be detected by Raman microscopy in specific spots of the sample but not by XPS. Moreover, the small intensity of the

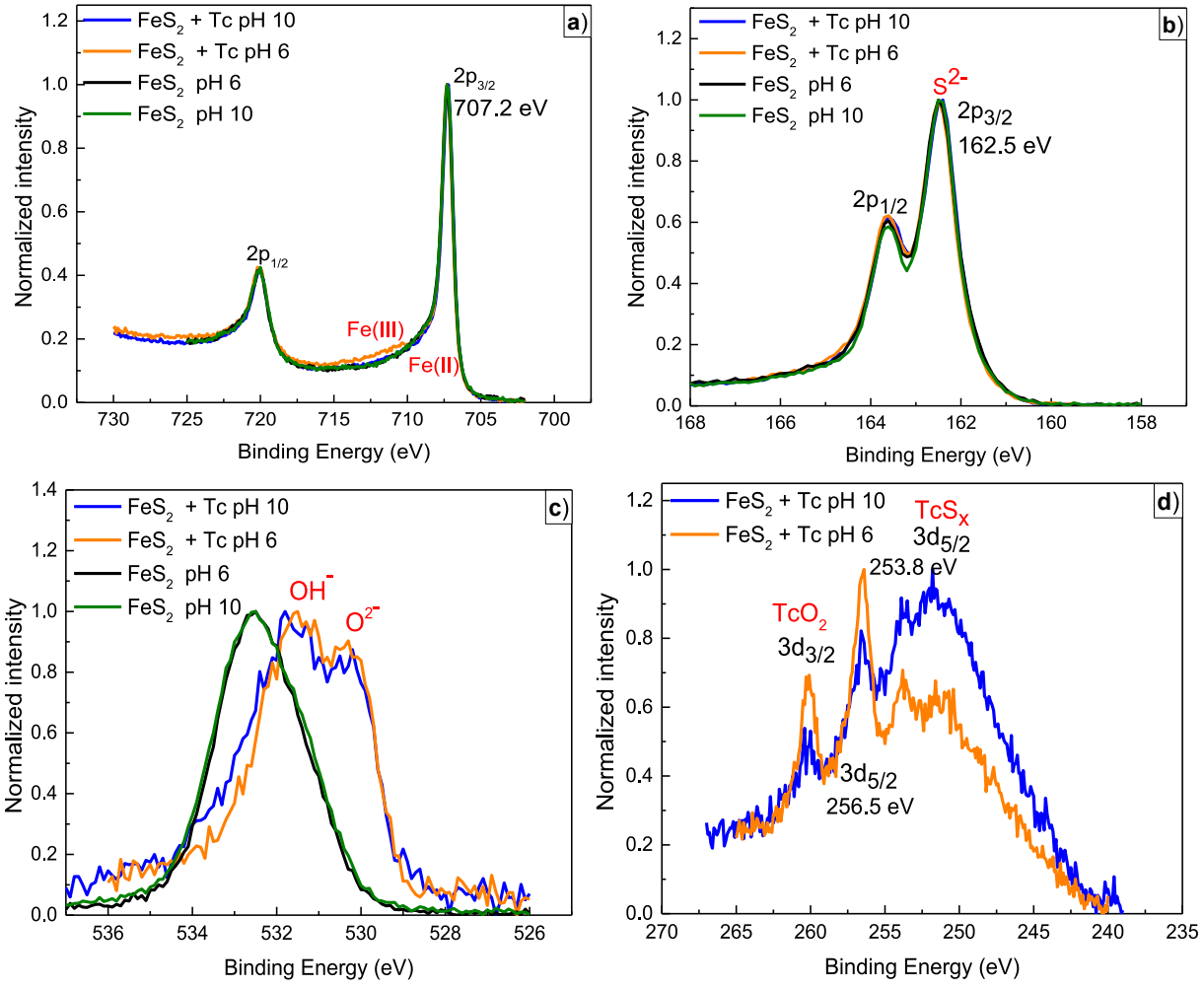

Fig. 3. XPS spectra of the synthetic FeS_2 after the reaction with Tc(VII) ([Tc] = 1000 ppm) at pH 6.0 and 10.0. a) Fe 2p. b) S 2p. c) O 1s. d) Tc 3d. Tc 3d elemental lines are superimposed by the broad loss line of S 2s.

band at 993 cm^{-1} in Fig. 2 portrays the low concentration of sulfate present in the sample.

The O *1s* spectra (Fig. 3c) of the pure synthetic FeS_2 presents a signal around 532.3 eV that could be assigned to adsorbed water, which has already been reported in literature for FeS_2 (Knipe et al., 1995). After the interaction with technetium, the samples at both pH 6.0 and 10.0 display the formation of similar proportions of OH^- and O^{2-}. The Tc *3d* spectra of the solids at pH 6.0 and 10.0 are presented in Fig. 3d. Due to the low concentration of Tc in the experiments the speciation by XPS can only be performed by the Tc *3d* main lines. The presence of TcO_2 at both pH values is indicated by the Tc $3d_{5/2}$ peak at 256.5 eV, which is close to the reference value 256.8 eV (NIST, 2012). The peak intensity suggests that formation of TcO_2 is favored at pH 6.0.

More intriguing are the Tc $3d_{5/2}$ peaks around 254 eV, whose binding energy is close to the reference binding energy for Tc(0) (253.9 eV (Gerasimov et al., 1982)). But it is preferably assigned to TcS_x or Tc-S-Fe bonding because the complete reduction to metallic technetium is not probable, as can be seen in the next paragraphs with the speciation calculations. A similar situation is noted in the Fe *2p* spectra, where the binding energy of Fe $2p_{3/2}$ at 707.2 eV (Fig. 3a) is close to the reference values of FeS_2 at 707.3 eV (NIST, 2012) and Fe(0) at 707.0 eV (Moulder et al., 1995) but it is assigned FeS_2 as it makes more chemical sense according to the sample. Although a reference of the Tc *3d* binding energy for TcS_2 could not be found, the Tc $3d_{5/2}$ line of Tc_2S_7 has a binding energy of around 254.8 eV (Gerasimov et al., 1984), which is close to that of the peaks around 254 eV in Fig. 3c. In consequence, the peaks at 254 eV were assigned to the formation of TcS_x–like species that seem to be more abundant as the pH becomes more alkaline. Such species were not detected by the S *2p* spectra due to the low concentration of technetium. In section 3.1, it was suggested that TcS_x species could passivate the mineral making the Tc reduction slower. Surface complexes might be formed, too, working as transient phases in the total redox process. Further studies are needed to gain deeper insight.

Fig. S2 in the SI shows the speciation diagrams of Tc reduction in presence of Fe^{2+} and/or S^{2-}. The performed calculations predict a quantitative Tc(VII) reduction to TcO_2 from pH 4.5 to pH 10.5. The Tc (VII) reduction by Fe^{2+} shows that main Fe(II) species in solution are Fe^{2+} at pH < 7.0 and for pH > 7.0 $Fe(OH)^+$ and $Fe(OH)_2$. For Fe(III) the main species formed are hematite at pH < 6.5 and magnetite at pH > 6.5 (SI Fig. S2a). In the case of the Tc reduction promoted by S^{2-}, the main S (II) species are HS^- throughout the entire pH range evaluated and the sulfur oxidation products are $S_{(cr)}$ at pH < 5.0 and SO_4^{2-} for pH > 5.0 (SI Fig. S2b).

In contrast, when the reduction of Tc(VII) is calculated in presence of both Fe^{2+} and S^{2-} (SI Fig. S2c), the formation of two solids, i.e. pyrite and mackinawite, and the presence of $Fe^{2+}_{(aq)}$, $FeOH^+_{(aq)}$ and $HS^-_{(aq)}$ are favored while the amount of Fe(III) and oxidized sulfur species represent a minority. This is related to the fact that Fe^{2+} and S^{2-} concentration are respectively 20 and 40 times higher than Tc and thus the main species found are Fe(II) and S(-II), whereas the formation of Fe and S oxidized products is low in comparison. These set up conditions might not be representative for a realistic scenario. However, when Fe^{2+} and SO_4^{2-} are in solution at pH > 7.0 the formation of $FeSO_4$ is favored (Hemingway et al., 2002). Even though these calculations need to be evaluated carefully since Tc homoreduction (i.e. in solution) by Fe^{2+} and S^{2-} coming from an assumed 1% FeS_2 dissolution is assumed, they support the Raman spectra obtained for the solids after interaction with Tc.

In summary, there is a clear effect of the marcasite on the technetium immobilization when compared with the previous results obtained with pure pyrite (Rodríguez et al., 2020). Not only the overall process is slower but also the Tc retention is incomplete at pH 10.0, which is a result of the change of the predominant redox active element (sulfur instead of iron).

3.3. Re-oxidation experiments

The initial concentration of Tc was 5 μM and the systems were left to interact for 14 days, after which the concentration of Tc in solution became 0.28 μM at pH 6.0 and 1.13 μM at pH 10.0. In order to estimate the amount of oxygen necessary to oxidize the synthetic FeS_2, the oxidation rates previously published for marcasite (Rinker et al., 1997) and pyrite (Williamson and Rimstidt, 1994) were used. Assuming that the mineral was entirely marcasite, the 0.065 g used for the re-oxidation experiments would need around 10 s to be fully oxidized whereas if the sample was constituted only by pyrite, it would need around 6 days. Even though these calculated times should be carefully considered as the FeS_2 oxidation rate should be affected by the presence of Tc(VII) as an oxidizing agent, they allow us to conclude that the time of the experiment was appropriate to observe Tc(IV) re-oxidation. Moreover, the concentration of oxygen required was rapidly reached since the opened tubes were shaken for 1 h, then closed and left under constant agitation for the entire experiment and they were opened several times for pH adjusting on the first days and for sampling during the following two months.

Fig. 4 shows the results of the re-oxidation experiments. The batch experiments from Fig. 4a depict the interesting fact that after the suspension at pH 10.0 was in contact with ambient atmosphere, the technetium concentration in solution was significantly lower (0.48 μM) than before the opening of the tube (1.13 μM). It is important to bear in mind that marcasite is much more reactive than pyrite and when it is exposed to oxidizing conditions, it rapidly generates H_2SO_4 (Rickard, 2012). This does not only explain the impossibility of maintaining the pH at 6.0 or 10.0 (section 2.5), but is also responsible for the further reduction of the Tc(VII) that was still in the suspension before the entry of oxygen at pH 10.0. The concentration of technetium in both suspensions remained below 1 μM for 50 days. In the last point of the re-oxidation experiments (64 days in Fig. 4a), it is apparent that the re-oxidation begins and it is more favorable in the suspension initially set at pH 6.0 than at pH 10.0. This behavior is very similar to the one found for pure pyrite (Rodríguez et al., 2020). The slower re-oxidation at pH 10.0 indicates that the Tc (IV)-species bond with the mineral is stronger, suggesting surface complexation at pH 6.0 and incorporation or co-precipitation at pH 10.0.

Fig. 4b shows the Raman spectra of the two Tc loaded-solids after 50 days under ambient atmosphere. The two solids have the same chemical identity, consisting of a mixture of the initial mineral (marcasite-pyrite 60:40) and sulfur in solid state, whose presence was confirmed by XRD of both solids (Fig. 4c) and supported by the speciation calculations (SI Fig. S2). This means that the initial pH does not play a role on the speciation after the system interacts with oxygen, most likely due to H_2SO_4 production.

The results presented here show that the presence of marcasite along with pyrite in a nuclear waste repository will prevent the re-mobilization of technetium due to the production of H_2SO_4 triggered by the presence of O_2 and the subsequent formation of elemental sulfur. The oxidation of marcasite is associated to the reduction of the Tc(VII) remaining in solution. Our results suggest that Tc will be immobilized as Tc(IV) until all the marcasite has been consumed, which would considerably limit a technetium distribution within the repository near and far field even if Tc(VII) reduction is not complete.

4. Conclusions

The immobilization of ^{99}Tc(VII) by a synthesized FeS_2, presenting a mixture of marcasite and pyrite (60:40) was studied. It was found that 100% of Tc(VII) is removed from solution after 7 days of interaction at 6.0 < pH ≤ 9.0. The Pourbaix diagram confirms that the initial step of the immobilization is the reduction of Tc(VII) to Tc(IV) at all the working pH values. At pH < 6.0 the Tc removal is incomplete due to the solubility of the synthesized FeS_2, as the reduction of Tc(VII) is less

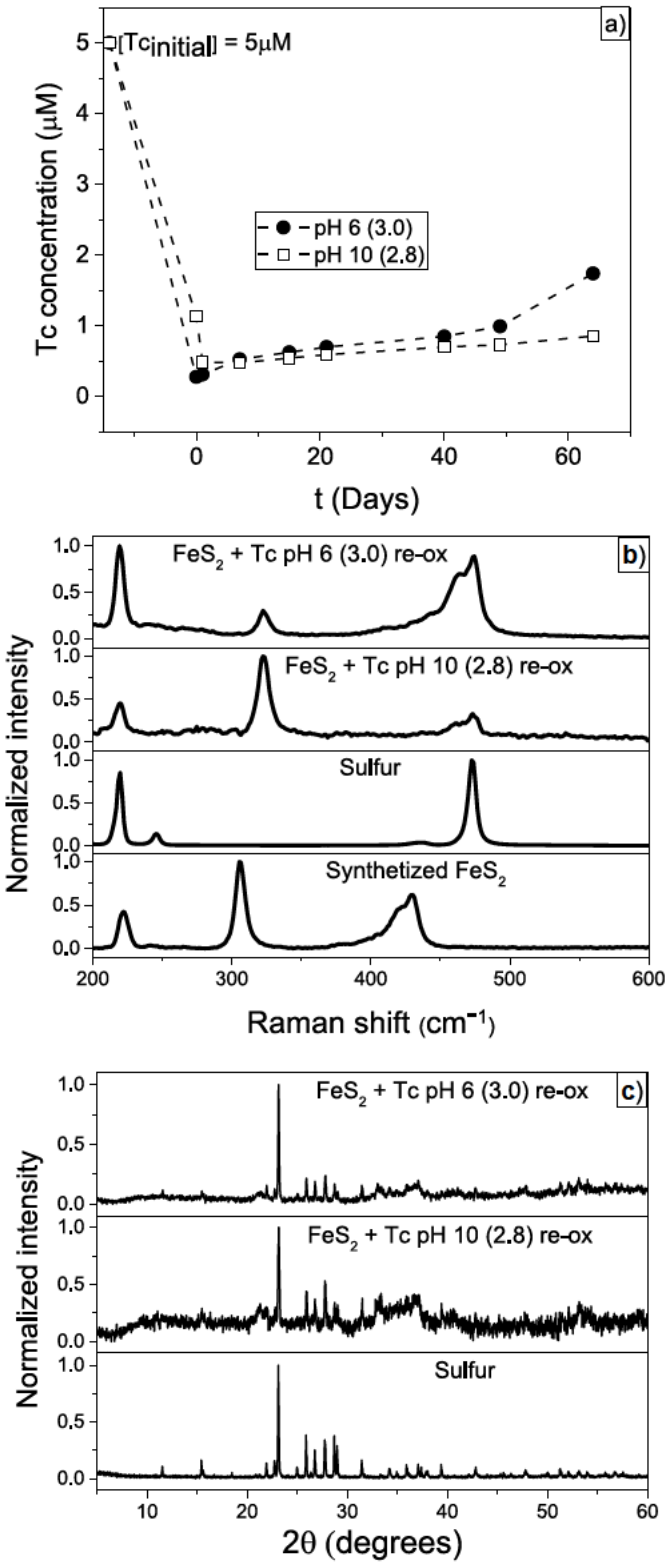

Fig. 4. Evaluation of Tc re-oxidation (re-ox) experiments at different pH values ($pH_{initial}$ = 6.0 and 10.0; pH_{air} = 3.0 and 2.8, respectively). a) Tc concentration in suspension for 70 days in ambient atmosphere. Dashed lines are shown to guide the eye. b) Raman spectra of the solids at $pH_{initial}$ 6.0 and 10.0 after 60 days of exposition to ambient atmosphere. The Raman spectra of the pure synthetic FeS_2 and sulfur (reference R040135) are shown as reference (Lafuente et al., 2016). c) XRD of the solids at $pH_{initial}$ 6.0 and 10.0 after 60 days of exposition to ambient atmosphere. The XRD of sulfur (reference R040135) are shown as reference (Lafuente et al., 2016).

efficient when Fe^{2+} is in solution. The spectroscopic analysis revealed that Fe(II) acts as the reducing agent at pH 6.0, producing hematite on which Tc(IV) sorption is feasible. These results are comparable to pure pyrite (Rodríguez et al., 2020). The behavior of the synthesized FeS_2 at pH 10.0 is different to pure pyrite and very surprising. Here, the Raman spectra indicated the formation of a $Fe(II)SO_4$ like mineral, implying that the reducing agent in that case was S^{2-}, which is a consequence of the higher reactivity of marcasite and might be an explanation for the incomplete Tc removal at this pH. Previous works with mackinawite, FeS (Yalçıntaş et al., 2016b), and in the presence of microorganisms (Pearce et al., 2018) have shown that, in general, after the reduction of Tc(VII) the formation of TcS_x compounds and polysulfides is observed. To our knowledge, our work provides new insights into the formation of sulfate minerals after the reduction of Tc(VII), highlighting the importance of further studies of the interaction of technetium with sulfur and other sulfur minerals like galena or chalcopyrite.

Even though the presence of marcasite makes the overall Tc retention less efficient when compared with pure pyrite, the re-oxidation experiments showed that the production of H_2SO_4 under ambient atmosphere leads to the immobilization of the technetium that was not retained by the synthesized FeS_2. In a realistic scenario, the oxidation of marcasite will promote the Tc(VII) reduction, which will favor Tc retardation due to the formation of less mobile Tc(IV) species.

As stated before, pyrite and marcasite are commonly misidentified and confused. This is a significant problem for the modeling of their ability to immobilize contaminants in the environment, which is especially important for most prominent redox-sensitive actinides and fission products in the context of a nuclear waste repository. This study shows the crucial role of the crystalline structure in the retention mechanism of technetium and opens the door to further comparisons of the scavenging ability of other polymorphs, like hematite and maghemite. Likely, data sets of other environmental pollutants, e.g. Se, As, Cd need a careful revision with respect to polymorphism.

CRediT author statement

Diana M. Rodríguez: Formal analysis, Investigation, Writing - Original Draft. **Natalia Mayordomo Herranz:** Formal analysis, Investigation, Writing - Review & Editing. **Dieter Schild:** Formal analysis, Writing - Review & Editing. **Salim Shams:** Formal analysis, Writing - Review & Editing. **Vinzenz Brendler:** Conceptualization, Writing - Review & Editing, Supervision, Project administration. **Katharina Müller:** Conceptualization, Writing - Review & Editing, Supervision, Project administration. **Thorsten Stumpf:** Conceptualization, Writing - Review & Editing, Supervision.

Declaration of competing interest

The authors declare that they have no known competing financial interests or personal relationships that could have appeared to influence the work reported in this paper.

Acknowledgments

This work was supported by the German Federal Ministry of Economic Affairs and Energy (VESPA II joint project; 02E11607B).

We are very grateful to Susana Jiménez, Stephan Weiβ and Carola Eckardt for their help in the laboratory.

Appendix A. Supplementary data

Supplementary data to this article can be found online at https://doi.org/10.1016/j.chemosphere.2021.130904.

References

Baumann, A., Gaona, X., Yalçıntaş, E., Dardenne, K., Prüßmann, T., Rothe, J., Duckworth, S., Altmaier, M., Geckeis, H., 2018. Appl. Geochem. 98, 321–330.
Baumer, T., Hixon, A.E., 2018. J. Environ. Radioact. 195, 20–25.
Bildstein, O., Trotignon, L., Perronnet, M., Jullien, M., 2006. Phys. Chem. Earth, Parts A/B/C 31, 618–625.
Boglaienko, D., Levitskaia, T.G., 2019. Environ. Sci. Nano 6, 3492–3500.
Boglaienko, D., Qafoku, O., Kukkadapu, R.K., Kovarik, L., Katsenovich, Y.P., Cherkasov, D.E., Emerson, H.P., Levitskaia, T.G., 2021. Environ. Sci. Nano 8, 97–109.
Bonnissel-Gissinger, P., Alnot, M., Ehrhardt, J.-J., Behra, P., 1998. Environ. Sci. Technol. 32, 2839–2845.
Cartledge, G.H., 1955. Corrosion 11, 23–30.
Cartledge, G.H., 1971. J. Electrochem. Soc. 118, 1752–1758.
Cui, D., Eriksen, T.E., 1996a. Environ. Sci. Technol. 30, 2259–2262.
Cui, D., Eriksen, T.E., 1996b. Environ. Sci. Technol. 30, 2263–2269.
De Craen, M., Van Geet, M., Wang, L., Put, M., 2004. Phys. Chem. Earth, Parts A/B/C 29, 91–103.
Environmental Protection Agency, 2000. National Primary Drinking Water Regulations: Radionuclides.
Gaucher, E., Robelin, C., Matray, J.M., Négrel, G., Gros, Y., Heitz, J.F., Vinsot, A., Rebours, H., Cassagnabère, A., Bouchet, A., 2004. Phys. Chem. Earth, Parts A/B/C 29, 55–77.
Gerasimov, V.N., Zelenkov, A.G., Kulakov, V.M., Pchelin, V.A., V Sokolovskaya, M., Soldatov, A.A., V Chistyakov, L., 1982. J. Exp. Theor. Phys. 55, 205–208.
Gerasimov, V.N., Zelenkov, A.G., Kulakov, V.M., Pchelin, V.A., Sokolovskaya, M.V., Soldatov, A.A., Chistyakov, L.V., 1984. J. Exp. Theor. Phys. 59, 683–688.
Gorski, C.A., Edwards, R., Sander, M., Hofstetter, T.B., Stewart, S.M., 2016. Environ. Sci. Technol. 50, 8538–8547.
Grenthe, I., Gaona, X., Plyasunov, A.V., Rao, L., Runde, W.H., Grambow, B., Konings, R.J. M., Smith, A.L., Moore, E.E., 2020. Second Update on the Chemical Thermodynamics of Uranium, Neptunium, Plutonium, Americium and Technetium. OECD Nuclear Energy Agency Data Bank, Boulogne-Billancourt, France.
Gu, P., Zhang, S., Li, X., Wang, X., Wen, T., Jehan, R., Alsaedi, A., Hayat, T., Wang, X., 2018. Environ. Pollut. 240, 493–505.
Hanesch, M., 2009. Geophys. J. Int. 177, 941–948.
Hemingway, B.S., Seal, R.R., Chou, I.-M., 2002. Thermodynamic Data for Modeling Acid Mine Drainage Problems: Compilation and Estimation of Data for Selected Soluble Iron-Sulfate Minerals Open-File Report 02-161. U.S. Geological Survey.
Herbert, R., Kulke, P.W., Shepherd, R.T.H., 1965. Postgrad. Med. 41, 656–662.
Hess, N.J., Xia, Y.X., Rai, D., Conradson, S.D., 2004. J. Solut. Chem. 33, 199–226.
Hiemenz, P.C., Rajagopalan, R., 1997. Principles of Colloid & Surface Chemistry, third ed. Taylor & Francis, New York.
Huo, L., Xie, W., Qian, T., Guan, X., Zhao, D., 2017. Chemosphere 174, 456–465.
Icenhower, J.P., Qafoku, N.P., Zachara, J.M., Martin, W.J., 2010. Am. J. Sci. 310, 721–752.
Johnson, I.E., Chatterjee, S., Hall, G.B., Burton, S.D., Campbell, E.L., Conroy, M.A., Du, Y., Fujimoto, M.S., Varga, T., Kruger, A.A., Levitskaia, T.G., 2018. Environ. Sci. Nano 5, 890–903.
Khasanova, A.B., Shcherbina, N.S., Kalmykov, S.N., Teterin, Y.A., Novikov, A.P., 2007. Radiochemistry 49, 419–425.
King, F., 2013. A Review of the Properties of Pyrite and the Implications for Corrosion of the Copper Canister Technical Report TR-13-19. Svensk Karnbranslehantering AB, Stockholm, Sweden.
Knipe, S.W., Mycroft, J.R., Pratt, A.R., Nesbitt, H.W., Bancroff, G.M., 1995. Geochem. Cosmochim. Acta 59, 1079–1090.
Lafuente, B., Downs, R.T., Yang, H., Stone, N., 2016. Highlights in Mineralogical Crystallography. De Gruyter, Berlin, pp. 1–30.
Lee, M.S., Um, W., Wang, G., Kruger, A.A., Lukens, W.W., Rousseau, R., Glezakou, V.A., 2016. Nat. Commun. 7, 1–6.
Lemire, R.J., Berner, U., Musikas, C., Palmer, D.A., Taylor, P., Tochiyama, O., 2013. Chemical Thermodynamics of Iron. Part 1, vol. 13a. OECD Nuclear Energy Agency Data Bank, Paris, France.
Lemire, R.J., Palmer, D.A., Schlenz, H., Taylor, P., 2019. Chemical Thermodynamics of Iron. Part 2. OECD Nuclear Energy Agency Data Bank, Boulogne-Billancourt, France.
Levitskaia, T.G., Chatterjee, S., Pence, N.K., Romero, J., Varga, T., Engelhard, M.H., Du, Y., Kovarik, L., Arey, B.W., Bowden, M.E., Walter, E.D., 2016. Environ. Sci. Nano 3, 1003–1013.
Li, F., Tao, L., Feng, C., Li, X., Sun, K., 2009. Environ. Sci. Technol. 43, 3656–3661.
Li, Y., Tian, X., Liang, J., Chen, X., Ye, J., Liu, Y., Liu, Y., Wei, Y., 2020. Environ. Pollut. 264, 114804.
Lieser, K.H., Bauscher, C., 1987. Radiochim. Acta 42, 205–213.
Limousin, G., Gaudet, J.-P., Charlet, L., Szenknect, S., Barthès, V., Krimissa, M., 2007. Appl. Geochem. 22, 249–275.
Mayordomo, N., Rodríguez, D.M., Schild, D., Molodtsov, K., Johnstone, E.V., Hübner, R., Shams Aldin Azzam, S., Brendler, V., Müller, K., 2020. J. Hazard Mater. 388, 122066.
Meena, A.H., Arai, Y., 2017. Environ. Chem. Lett. 15, 241–263.
Moulder, J.F., Stickle, W.F., Sobol, P.E., Bomben, K.D., 1995. Handbook of X-Ray Photoelectron Spectroscopy. ULVAC-PHI, Inc. Japan, Physical Electronics USA, Inc., Eden Prairie, USA.
NIST, 2012. NIST X-Ray Photoelectron Spectroscopy Database Version 4.1. National Institute of Standards and Technology (NIST), Gaithersburg, USA.
Pearce, C.I., Icenhower, J.P., Asmussen, R.M., Tratnyek, P.G., Rosso, K.M., Lukens, W.W., Qafoku, N.P., 2018. ACS Earth Sp. Chem. 2, 532–547.
Pearce, C.I., Moore, R.C., Morad, J.W., Asmussen, R.M., Chatterjee, S., Lawter, A.R., Levitskaia, T.G., Neeway, J.J., Qafoku, N.P., Rigali, M.J., Saslow, S.A., Szecsody, J. E., Thallapally, P.K., Wang, G., Freedman, V.L., 2019. Sci. Total Environ. 716, 132849.
Perrier, C., Segrè, E., 1937. Nature 140, 193–194.
Rard, J., Rand, M., Anderegg, G., Wanner, H., 1999. Chemical Thermodynamics of Technetium. North Holland Elsevier Science Publishers B. V., Amsterdam, The Netherlands.
Rickard, D., 2012. Sulfidic Sediments and Sedimentary Rocks. Elsevier B.V, Amsterdam.
Rinker, M.J., Nesbitt, H.W., Pratt, A.R., 1997. Am. Mineral. 82, 900–912.
Rodríguez, D.M., Mayordomo, N., Scheinost, A.C., Schild, D., Brendler, V., Müller, K., Stumpf, T., 2020. Environ. Sci. Technol. 54, 2678–2687.
Schulte, E.H., Scoppa, P., 1987. Sci. Total Environ. 64, 163–179.
Seah, M.P., Gilmore, I.S., Beamson, G., 1998. Surf. Interface Anal. 26, 642–649.
Shi, K., Hou, X., Roos, P., Wu, W., 2012. Anal. Chim. Acta 709, 1–20.
Sun, Y., Lv, D., Zhou, J., Zhou, X., Lou, Z., Baig, S.A., Xu, X., 2017. Chemosphere 185, 452–461.
Talikka, M., 2005. Geological Mapping of the ONKALO Open Cut. Posiva Oy, Olkiluoto, Finland.
van der Lee, J., de Wint, L., 1999. Chess Tutorial and Cookbook. Updated for version 3.0. Ecole des Mines de Paris, Fontainebleau.
Wang, T., Qian, T., Huo, L., Li, Y., Zhao, D., 2019. Environ. Pollut. 255, 112992.
Williamson, M.A., Rimstidt, J.D., 1994. Geochem. Cosmochim. Acta 58, 5443–5454.
Xu, N., Christodoulatos, C., Braida, W., 2006. Chemosphere 62, 1726–1735.
Yalçıntaş, E., Gaona, X., Altmaier, M., Dardenne, K., Polly, R., Geckeis, H., 2016a. Dalton Trans. 45, 8916–8936.
Yalçıntaş, E., Scheinost, A.C., Gaona, X., Altmaier, M., 2016b. Dalton Trans. 45, 17874–17885.
Yao, X., Xia, F., Deditius, A.P., Brugger, J., Etschmann, B.E., Pearce, M.A., Pring, A., 2020. Contrib. Mineral. Petrol. 175, 27.
Zachara, J.M., Heald, S.M., Jeon, B.-H., Kukkadapu, R.K., Liu, C., McKinley, J.P., Dohnalkova, A.C., Moore, D.A., 2007. Geochem. Cosmochim. Acta 71, 2137–2157.

Reductive immobilization of ^{99}Tc(VII) by FeS_2: the effect of marcasite

Diana M. Rodríguez [1], Natalia Mayordomo [1], Dieter Schild [2], Salim Shams Aldin Azzam [1], Vinzenz Brendler [1], Katharina Müller [1*], Thorsten Stumpf [1]*

[1] Helmholtz-Zentrum Dresden – Rossendorf (HZDR), Institute of Resource Ecology, Bautzner Landstraße 400, 01328 Dresden, Germany

[2] Karlsruhe Institute of Technology (KIT), Institute for Nuclear Waste Disposal, Hermann-von-Helmholtz-Platz 1, 76344 Eggenstein-Leopoldshafen, Germany

* Corresponding author: n.mayordomo-herranz@hzdr.de (N. Mayordomo, Phone: +49 351 260 2076), k.mueller@hzdr.de (K. Müller, Phone: +49 351 260 2439)

Catalogue of Supporting Information:

Reductive immobilization of ^{99}Tc(VII) by FeS_2: the effect of marcasite (SI)

Table S1. Conditions of the batch sorption experiments

Experiment	Kinetics	pH effect	Isotherm
$[Tc(VII)]_0$ (M)	5×10^{-6}	5×10^{-6}	$2\times10^{-7} – 2\times10^{-3}$
pH	6.5	4.5 - 10.0	6.5
Contact time (days)	1 – 45	14	14

Reductive immobilization of ^{99}Tc(VII) by FeS_2: the effect of marcasite (SI)

Mineral characterization

Figure S1a shows the powder XRD of the matt-black powder obtained. The diffractogram shows that the synthesis yielded a mixture of marcasite (orthorhombic FeS_2) and pyrite (cubic FeS_2) by comparison with the references available in the RRUFF™ database[1] (References R060882 and R050190). A whole powder pattern fitting (WPPF) was performed with the data analysis software (PDXL: integrated X-ray powder diffraction software, Version 2.8.1.1) and it was found that the proportion between marcasite and pyrite is 60:40. Such proportion suits well the purpose of this study since the difference between the already known Tc removal by pure pyrite[2] and the Tc removal obtained by this mixture of minerals could be attributed to the higher amount of marcasite present.

The results of ζ-potential measurements are presented in Figure S1b. The pH_{IEP} was determined at 7.4, which indicates that the synthesized iron sulfide presents some Fe(III) moieties on the surface, i.e. the surface is partly oxidized.[3,4] We refrained from applying an acid wash to the mineral since the presence of Fe(III) is also to be expected on natural FeS_2 surfaces.[5] Furthermore, in the diffractogram (Figure S1a) no peaks can be attributed to other mineral phases apart from pyrite and marcasite, indicating that the contribution of Fe(III) is not significant. The micrographs depicted in Figures S1c and S1d show that the solid obtained is a mixture of cubic (pyrite) and orthorhombic (marcasite) FeS_2 crystals, being the orthorhombic particles more abundant. The marcasite crystals present a particle size around 1 – 2 μm, while for the pyrite ones it is around 0.5 and 1 μm.

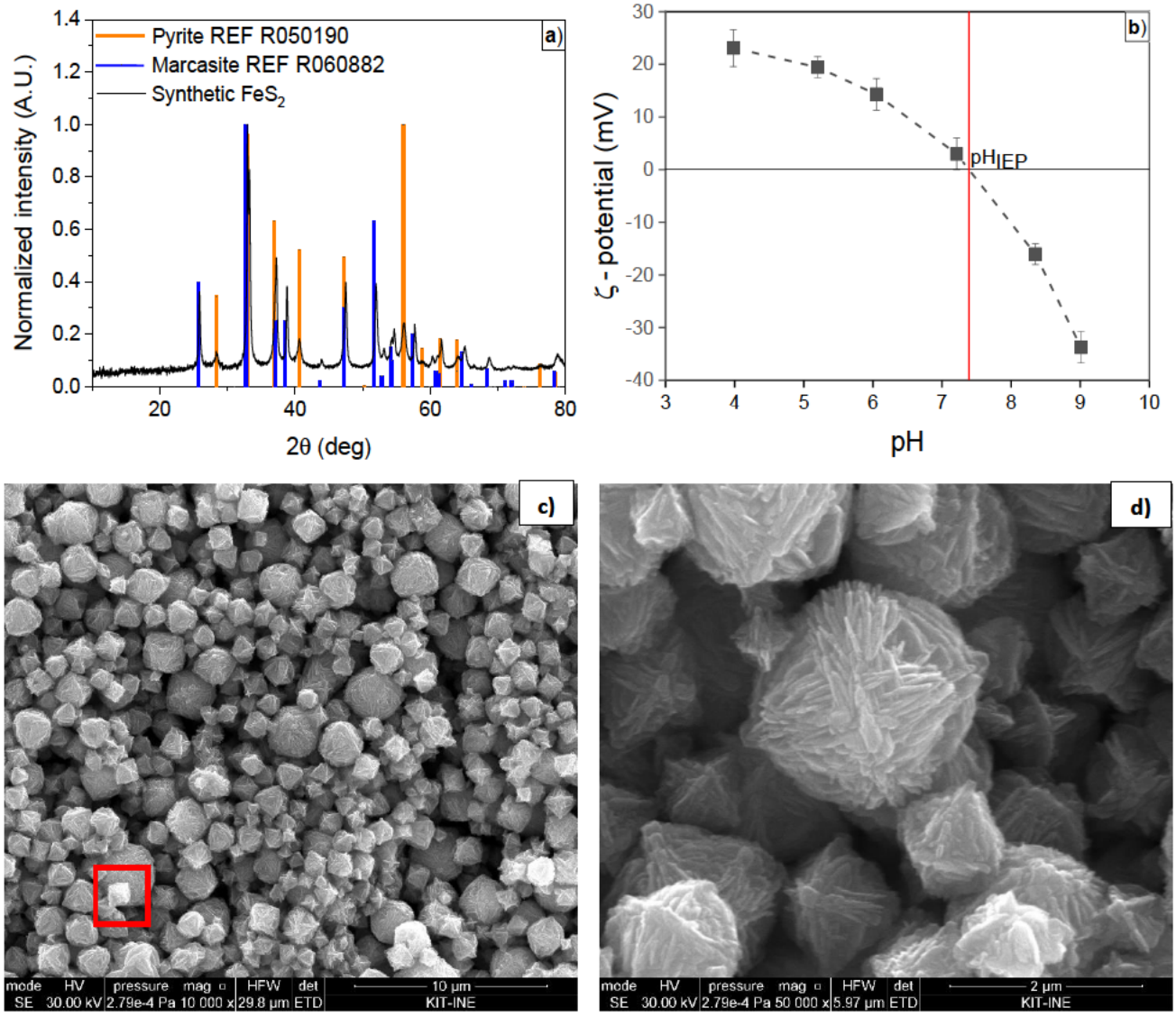

Figure S1. Characterization of the synthesized FeS_2 sample. a) Powder XRD. References of pyrite and marcasite were added for comparison.[1] b) ζ-potential measurements for the determination of the isoelectric point. c) and d) SEM secondary electron images at different magnifications. Highlighted in red: cubic crystal.

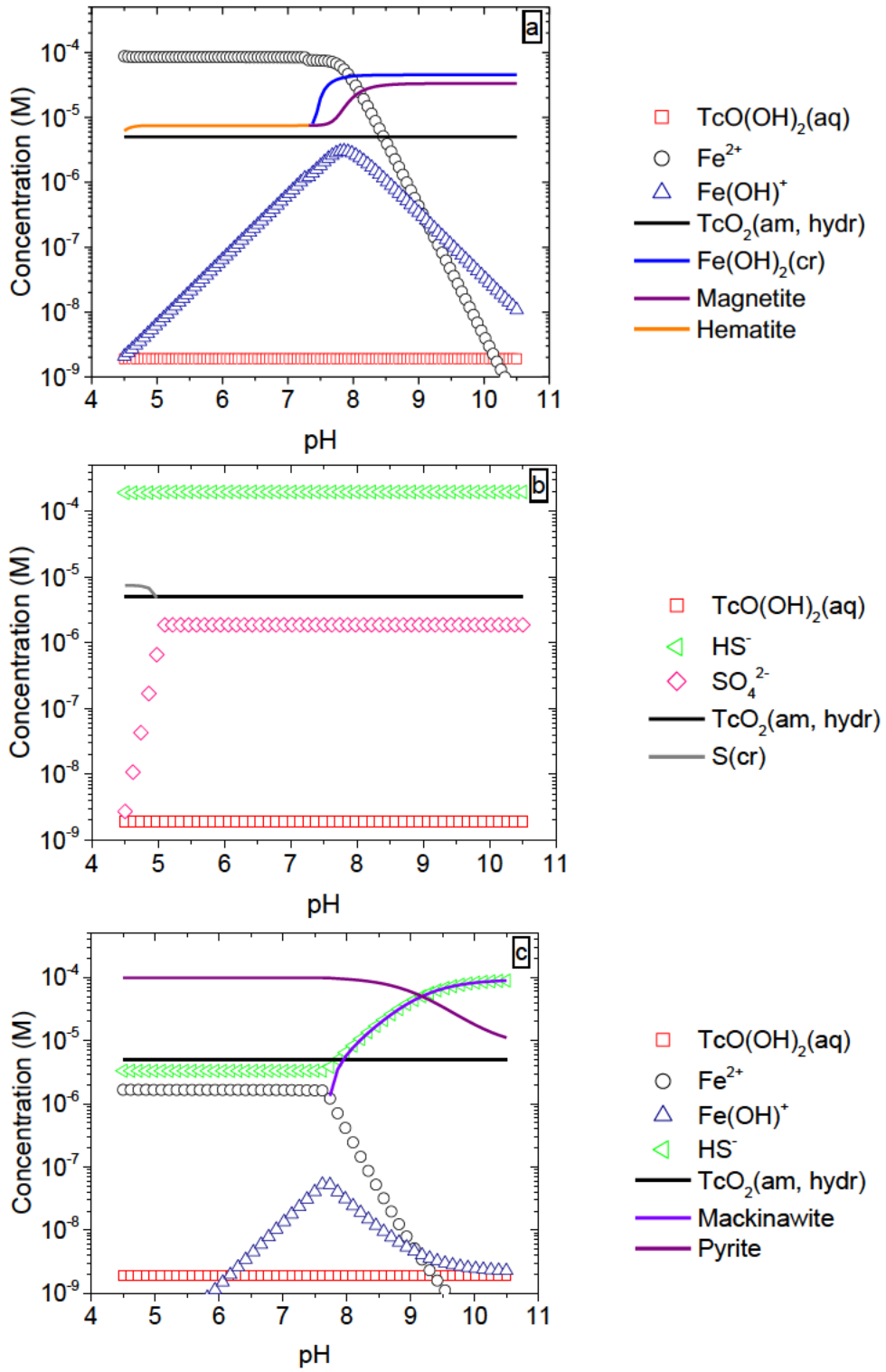

Figure S2. Speciations calculated as a function of pH. Tc(VII) reduction in the presence of a) Fe^{2+}, b) S^{2-}, c) both Fe^{2+} and S^{2-}. Initial boundary conditions: 0.1 mM Fe^{2+}, 0.2 mM S^{2-} and 5 µM TcO_4^-.The most recent NEA TDB was utilized for thermodynamic data of Fe[6,7] and Tc[8] as well as S.

SI References

1 B. Lafuente, R. T. Downs, H. Yan and N. Stone, in *Highlights in Mineralogical Crystallography*, De Gruyter, Berlin, 2015, pp. 1–30.

2 D. M. Rodríguez, N. Mayordomo, A. C. Scheinost, D. Schild, V. Brendler, K. Müller and T. Stumpf, *Environ. Sci. Technol.*, 2020, **54**, 2678–2687.

3 D. A. Kitchaev and G. Ceder, *Nat. Commun.*, 2016, **7**, 13799.

4 P. Bonnissel-Gissinger, M. Alnot, J.-J. Ehrhardt and P. Behra, *Environ. Sci. Technol.*, 1998, **32**, 2839–2845.

5 G. Hu, K. Dam-Johansen, S. Wedel and J. P. Hansen, *Prog. Energy Combust. Sci.*, 2006, **32**, 295–314.

6 R. J. Lemire, U. Berner, C. Musikas, D. A. Palmer, P. Taylor and O. Tochiyama, *Chemical Thermodynamics of Iron. Part 1*, OECD Nuclear Energy Agency Data Bank, Paris, France, 2013, vol. 13a.

7 R. J. Lemire, D. A. Palmer, H. Schlenz and P. Taylor, *Chemical Thermodynamics of Iron. Part 2*, OECD Nuclear Energy Agency Data Bank, Boulogne-Billancourt, France, 2019.

8 I. Grenthe, X. Gaona, A. V. Plyasunov, L. Rao, W. H. Runde, B. Grambow, R. J. M. Konings, A. L. Smith and E. E. Moore, *Second update on the chemical thermodynamics of uranium, neptunium, plutonium, americium and technetium*, OECD Nuclear Energy Agency Data Bank, Boulogne-Billancourt, France, 2020.